JOURNAL OF MATERIALS SCIENCE **40** (2005) 1685–1691

Co,Ni-base alloy thin films deposited by r.f. magnetron sputtering in Ar/N_2 atmosphere

M. LEONI, C. TOSI, P. SCARDI*
Dipartimento di Ingegneria dei Materiali e Tecnologie Industriali, Università di Trento, 38050 Mesiano (TN), Italy
E-mail: Paolo.Scardi@unitn.it

Phase composition and microstructure of CoNiCrAlY thin films deposited by r.f. Magnetron Sputtering in reactive Ar/N_2 atmosphere were determined by X-ray Diffraction. Three basic phases were observed, for increasing nitrogen partial pressure: (a) a nanocrystalline supersaturated solid solution of the alloy elements with *fcc* structure and interstitial nitrogen (up to 10–15%), with a sharp [111] fibre texture turning into a broad [200] component for increasing N_2 content; (b) an amorphous phase with nominal composition M_2N (with M as the alloy elements); and (c) a nanocrystalline nitride approaching the nominal composition MN. Nanocomposite coatings made of nanocrystalline *fcc* metal phase embedded in an amorphous matrix can be formed in a relatively narrow N_2 partial pressure range, whereas at high nitrogen content the thin films tend to form an increasing fraction of a nanocrystalline nitride in addition to the amorphous matrix.

Scratch test results are different for the various systems: thin films made of (a) behave as typical plastic metals, with an increased scratch test resistance for increasing N_2 content; amorphous (b) films show a very good scratch test behaviour and tend to fail in a plastic mode, with optimal properties for systems made of *fcc* metal nanocrystalline/amorphous nanocomposites; thin films with a high N_2 content tend to behave in a brittle way for increasing content of the nanocrystalline nitride phase.

1. Introduction

Extensive research activity in the last ten years demonstrated the possibility of obtaining a large variety of non-equilibrium microstructures and phase compositions in thin films produced by r.f. Magnetron Sputtering (rfMS). In particular, several studies were devoted to the production of nanocrystalline and amorphous thin films of metal alloys made of partly miscible or immiscible elements, deposited in chemically neutral (Ar) or in reactive (e.g., Ar/N_2) atmosphere [1–4].

The potential interest in the rfMS process relies on the possibility of producing thin films with new properties, markedly different from those of the corresponding equilibrium 'bulk' phases. Even more so considering nanocomposites that can be formed, for example, by combining nanocrystalline phases or by embedding nanocrystalline domains in an amorphous matrix [1–4]. These amorphous and nanocomposite thin films are known for the high hardness that can be obtained, frequently in conjunction with a plastic behaviour that cannot be found in traditional hard coatings [5].

It is now demonstrated that co-deposition of elements (from different targets or from alloy target) whose phase diagram presents a wide miscibility gap is a prerequisite for forming non-equilibrium nanocrystalline or amorphous phases. This tendency to form non-crystalline phases is further increased by the sputter deposition in a reactive atmosphere [3–5]. Co,Ni-base alloys, like those used in turbine applications (e.g., CoNiCrAlY), are good candidates to form non-equilibrium phases by rfMS. These materials in bulk or in powder form tend to separate in two phases (typically a mixture of α-γ metal phases) owing to the limited solubility of the components.

In a recent work we already demonstrated that amorphous thin films of a Co,Ni-base alloy can be deposited by rfMS in reactive Ar/N_2 atmosphere [5]. These amorphous thin films exhibit a relatively good hardness (as compared with conventional nitride coatings like TiN) coupled with a plastic behaviour and very good adhesion to metal substrates. In the present paper we investigate the structural features of thin films of a Co,Ni-base alloy deposited in reactive Ar/N_2 atmosphere, for deposition conditions ranging from pure Ar to pure N_2. This work is the basis to the following study (in progress) to assess (a) application as protective coatings, (b) thermal stability and (c) magnetic properties of the thin films.

*Author to whom all correspondence should be addressed.

2. Experimental

2.1. Specimen preparation

Coatings were deposited on two different kinds of substrates: (a) AISI D2 tool steel (1.55%C, 12.0%Cr, 0.7%Mo, 1%V, balance Fe-in weight) machined into $25 \times 12 \times 5$ mm^3 coupons, with a base micro-hardness of 770–820 HV (63–65 HRC) for the use in the scratch tests; (b) Silicon wafer ⟨h00⟩ for structural tests. Steel substrates were polished to a 6 μm finish by standard metallographic techniques, leading to an average surface roughness $R_a = 25 \pm 5$ nm. All substrates were cleaned first in acetone and then in absolute ethanol using an ultrasonic bath, and finally dried in nitrogen flux before placing in the deposition chamber.

Coatings were prepared by r.f. Magnetron Sputtering (Leybold Z400 unit working at 13.56 MHz), using planar targets (Ø 75 mm) placed 39 mm above the substrate holder. Pre-deposition procedures included a sputter cleaning of the substrate surface (for steel substrates only) by polarity inversion sputtering (back-sputtering, p_{Ar} $4 \times 10^{-1} \div 6 \times 10^{-1}$Pa, rf power 10 W for 2 min) and sputter cleaning of the target surface (p_{Ar} $4 \times 10^{-1} \div 6 \times 10^{-1}$Pa, rf power 100 W for 2 min). The residual gas pressure in the deposition chamber prior to deposition was $\sim 2 \times 10^{-4}$ Pa.

Depositions from a target of Co,Ni-base alloy (38.0%Co, 32%Ni, 21%Cr, 8%Al, 0.5%Y_2O_3-in weight) were done in argon/nitrogen atmosphere. Samples were produced at different Ar/N_2 ratios, maintaining a constant total pressure of 6×10^{-1}Pa and 100 W rf power. Table I reports nitrogen content of the deposition atmosphere and thickness, for all the samples produced in this study. Steel substrate surface temperature during sputter cleaning was kept below 100°C by a water cooling system, whereas during deposition the temperature did not exceed 250°C.

2.2. Characterization

X-ray Diffraction (XRD) patterns were collected in the usual Bragg-Brentano geometry using a Rigaku D-Max diffractometer, equipped with a graphite bent-crystal analyser and a Cu tube. In addition, $\theta/2\theta$-ψ maps were collected on the same samples by means of a Philips X'Pert MRD diffractometer using a 4-circle goniometer and a pseudo-parallel beam geometry based on a polycapillary lens in primary beam coupled with vertical collimators and a graphite flat-crystal analyser in the diffracted beam. Details on this geometrical set-up and on the use of the θ-2θ-ψ maps can be found elsewhere [6, 7]. Chemical composition was controlled by a LINK AN 10000 Energy Dispersive Spectroscopy (EDS) installed on a Cambridge Stereoscan S360 scanning electron microscope.

Coating thickness was measured using a DEKTAK3 profilometer. Adhesion was studied on the thin films deposited on steel substrates, using a commercial scratch tester (Revetest CSEM apparatus) fitted with a Rockwell C diamond stylus (cone apex angle 120°; tip radius 200 μm), acoustic emission (AE) sensor and a tangential force measuring system. In the scratch test a progressive load is applied to the surface of the coating by means of the stylus meanwhile the sample is displaced at a constant speed. The result of the scratch can be monitored during the test by acoustic emission and off line by optical observations. Generally a critical load is defined as the normal force at coating's failure and it can be used to compare the adhesion behaviour of different coatings. The value of critical load can be determined by measuring the distance between the start of the scratch and the delamination point as established using optical and acoustic emission observations.

TABLE I Nitrogen partial pressure (P_{N_2}), ratio to the total deposition pressure (0.6 Pa) (P_{N_2}/P_{TOT}) and thin film thickness

Substrate steel	P_{N_2} (Pa)	P_{N_2}/P_{TOT}	Thickness (μm)
MA	0.14×10^{-4}	0.233×10^{-4}	3.9
MB	0.23×10^{-2}	0.383×10^{-2}	3.6
MC	0.1×10^{-1}	0.167×10^{-1}	4
MD	0.4×10^{-1}	0.667×10^{-1}	3.7
ME	0.1	0.167	9.2
MF	0.2	0.333	2.5
MG	0.3	0.5	2.7
MH	0.5	0.833	2.7
MI	0.6	1	3
Silicon			
SA	0.14×10^{-4}	0.233×10^{-4}	2.9
SB	0.23×10^{-2}	0.383×10^{-2}	3.4
SC	0.6×10^{-2}	0.1×10^{-1}	3.4
SD	0.1×10^{-1}	0.167×10^{-1}	3.5
SE	0.18×10^{-1}	0.3×10^{-1}	3.4
SF	0.4×10^{-1}	0.667×10^{-1}	3.5
SG	0.85×10^{-1}	0.142	4.2
SH	0.3	0.5	3
SI	0.6	1	3

3. Results and discussion

3.1. Phase composition

X-ray diffraction patterns for samples deposited on silicon wafers are shown in Figs 1–3. To avoid interference with the substrate, data were collected with a 3° offset in addition to the θ value given by the usual $\theta/2\theta$ coupling condition; in this way, the strong single-crystal signal from the [h00] oriented substrates was excluded. Data are displayed in separate figures to better distinguish fine details in the patterns.

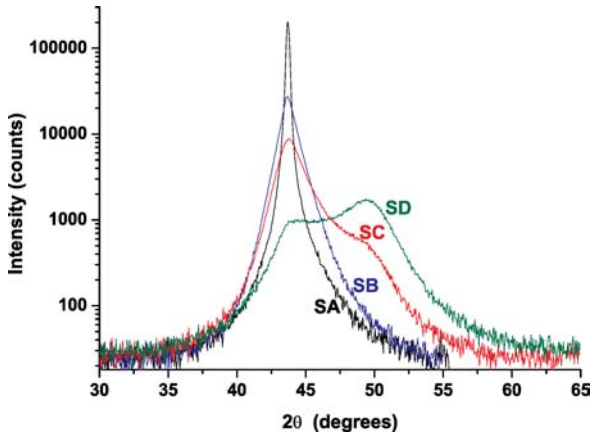

Figure 1 Low 2θ angle region of the X-ray diffraction patterns of the specimens SA, SB, SC and SD. Log scale is used, as to enhance the smaller details.

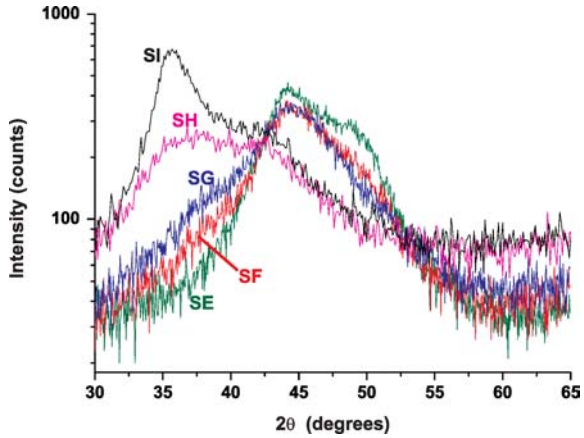

Figure 2 Low 2θ angle region of the X-ray diffraction patterns of the specimens SE, SF, SG, SH and SI. Log scale is used, as to enhance the smaller details.

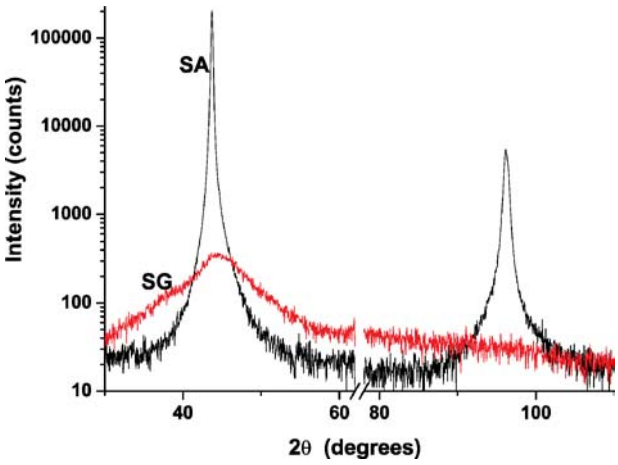

Figure 3 Comparison of the X-ray diffraction patterns of the specimens SA (crystalline) and SG (most likely amorphous). Log scale is used, as to enhance the weaker features in the pattern.

As expected from a previous study [5], thin films of Co,Ni-base alloy deposited in Ar give only an intense signal from the (hhh) planes of a *fcc* phase (Figs 1 and 3). Pole figures confirm the *fcc* metal structure with a strong [111] fibre texture [5], typical of many metallic films deposited by PVD techniques under non-epitaxial conditions. By increasing the nitrogen content (sample SB), XRD reflections become progressively broader, still keeping a predominant [111] texture. Starting from sample SC a 'shoulder' appears in correspondence of the (200) line expected position, whereas in sample SD the broad (200) reflection is more intense than the (111), pointing out an evolution in the thin film texture. In conclusion, all samples SA to SD (Fig. 1) appear as made of a polycrystalline, textured *fcc* metal phase, whose crystalline domain size tends to decrease with the N_2 content.

As shown in Fig. 2, a further increase in N_2 leads to markedly different systems. In fact, samples SE, SF and SG exhibit a broad diffraction signal that cannot be directly identified as a reflection from a crystalline phase. Differences with respect to the pattern of the textured *fcc* metal phase can be better appreciated in Fig. 3. Samples SE, SF, SG are most likely amorphous [5]. Even if crystalline, the domain size given by the profile width would be extremely small, of the order of ~1 nm or less [5]. In the pattern of sample SE it is still visible a 'shoulder' at the angular position of the (200) line of the *fcc* metal phase found for lower nitrogen content, possibly indicating that the sample is not entirely amorphous. In general, it cannot be excluded that in addition to the main amorphous phase a minor fraction of nanocrystalline metal phase is also present in these thin films.

For higher nitrogen contents, the system tends to form nitride phases. The pattern of sample SI (deposited in 100% N_2 atmosphere) shows two reflections, quite broad but still identifiable as the (111) and (200) peaks of a *fcc* nitride phase close to CoN. By modelling the two profiles the lattice parameter is $a_0 = 0.434$ nm, with respect to $a_0 = 0.4297$ nm for the CoN phase reported by the literature [8], a difference that can be justified by the presence of the other alloy elements and possible non-stoichiometric Co/N ratio. The broad profiles suggest the presence of a nanocrystalline phase. However, it is worth noting here that the presence of additional phases (nitrides or amorphous) in sample SI cannot be excluded on the basis of this XRD pattern.

Sample SH seems to be intermediate between the 'amorphous' SG and the nitride SI. The sample might therefore contain both phases, even if, also in this case, the evidence given by the powder pattern is not conclusive. Finally, with reference to Fig. 2, it can be recognised that sample SG shows a 'shoulder' on the low-angle tail of the broad reflection, which is probably related to a beginning of nitride phase formation.

To get a more clear picture of phase composition and texture we also collected $\theta/2\theta$-ψ maps. As shown in previous studies, if preferentially oriented, these thin film systems tend to exhibit a fibre-type texture [5]. As a consequence of the fibre symmetry, it is not necessary to collect traditional pole figures to study texture: orientations can be evaluated by collecting $\theta/2\theta$ patterns at different tilt angles (ψ) for a fixed in-plane sample rotation angle (ϕ) [6, 7]. In these $\theta/2\theta$-ψ maps, localised maxima (poles) point out the presence of preferred orientation, whereas random oriented polycrystalline or amorphous phases exhibit diffraction signals of constant intensity with the ψ-tilt. The maps can therefore be used to support the identification obtained by the powder patterns and to simultaneously evaluate fibre texture components.

$\theta/2\theta$-ψ maps for the samples deposited on Si wafers are shown in Fig. 4. Conventional $\theta/2\theta$ patterns like those of Figs 1–3 correspond to straight lines at zero ordinate in the maps of Fig. 4. Sample SA map (Fig. 4a) shows a maximum for $\psi = 0^\circ$ and 2θ corresponding to the (111) reflection of the *fcc* metal phase observed in Figs 1 and 3. Two further poles are at $\psi \approx 70.5^\circ$, nearly same 2θ as the main poles and at $\psi \approx 54.5^\circ$ for a 2θ corresponding to the (200) line. These observations are a clear indication that sample SA grew with (111) close packing planes parallel to the surface, so that the poles at $\psi \approx 70.5^\circ$ and $\approx 54.5^\circ$ are produced, respectively, by $(11\bar{1})$ and (002) planes. Similar observations can be made for sample SB and SC, even if poles become progressively broader with increasing N_2 content, pointing

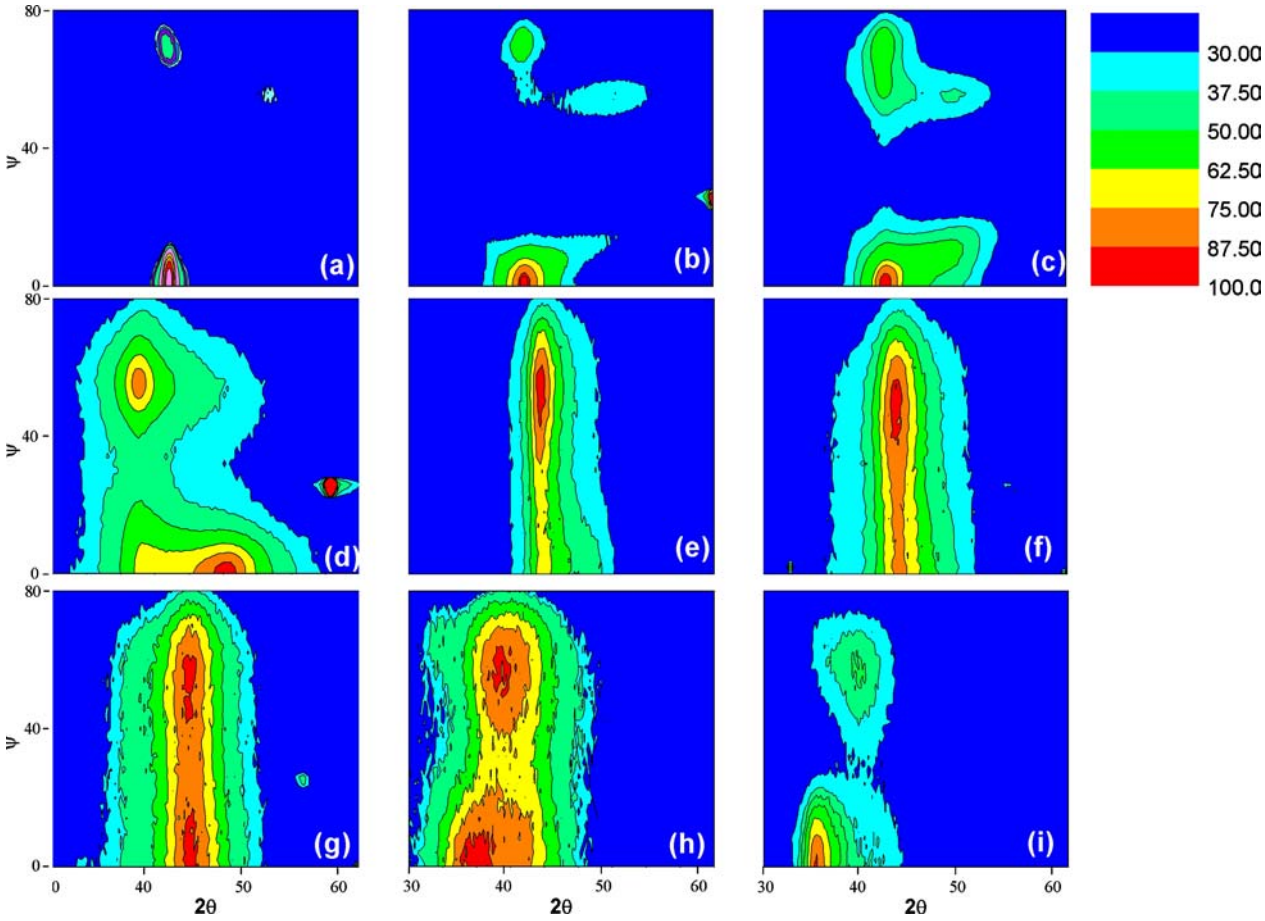

Figure 4 $\theta/2\theta$-ψ maps for the samples deposited on Si wafers: (a) SA, (b) SB, (c) SC, (d) SD, (e) SE, (f) SF, (g) SG, (h) SH, (i) SI.

out the presence of smaller crystallites (and/or higher lattice defect density) and less sharp [111] texture.

Sample SC shows some additional features that become more evident in sample SD. The latter (Fig. 4d) shows broad poles with a maximum for the (200) reflection at $\psi = 0°$. Additional poles are at $\psi \approx 54.5°$ and 2θ for the (111) line. Both poles extend to include a lower signal centred in positions close to those observed in sample SA. As a consequence, it can be concluded that sample SD still exhibits the *fcc* structure of samples SA-SC, but the main texture component is [200], with a secondary fibre component along [111]. The [200] component starts to appear in sample SC (cf. Figs 1 and 4c).

Maps SE, SF and SG (Figs 4e–g, respectively) show only a broad maximum close to (but not coinciding with) the (111) reflection, with a moderate variation of the intensity with the ψ-tilt. It is worth noting here that sample illumination, film thickness and geometry of the X-ray optics are responsible for a slight increase of the intensity from $\psi \approx 0°$ to $\psi \approx 60°$ and a more rapid decrease above $\psi \approx 60°$ [9]: the broad signals in these maps can therefore be considered as nearly constant for all ψ-tilts. This information strongly supports the results of the powder patterns that samples SE, SF and SG are amorphous. In sample SE (Fig. 4e) it is possible to see a residual of the (200) reflection at $\psi \approx 0°$, leading to the conclusion that these thin films may actually contain a secondary nanocrystalline phase.

Sample SI map shows features compatible with the presence of a nanocrystalline nitride phase (CoN-type) with some degree of [111] orientation. In fact, a broad pole is present at $\psi \approx 0°$, centred at the 2θ position observed in the powder pattern (Fig. 2) for the (111) peak of the nitride phase. This main pole includes a lower signal from the (200) planes. The distinctive evidence of texture is given by the broad pole at $\psi \approx 55°$ for a 2θ position close to that of the (200) reflection observed in the powder pattern (the 2θ position of the pole is shifted toward lower angles, most likely because of a residual tensile stress [6, 7]). However, the [111] texture in the nitride phase of sample SI is much broader than the sharp [111] texture in the metal phase of sample SA.

Finally, sample SH gives a map with features intermediate between SG and SI, so it is most likely made of two phases: an amorphous component and a nanocrystalline nitride. As indicated by the powder patterns (Fig. 2), nitrides tend to appear as secondary phases even for lower N_2 content, when the samples (e.g. SG) are predominantly amorphous.

All the above observations can be summarized in a non-equilibrium phase diagram, where the observed phases are reported as a function of the nitrogen fraction present in the deposition atmosphere. The diagram of Fig. 5 is conveniently positioned below the EDS results, giving the actual concentration of nitrogen in the thin films. As shown in Fig. 5, ranges of existence of the three phases—*fcc* metal phase (with [111] and [200] texture), amorphous phase and nanocrystalline nitride—overlap in regions where two phases were observed. The exact extension of these regions should be determined by further study of thin films produced

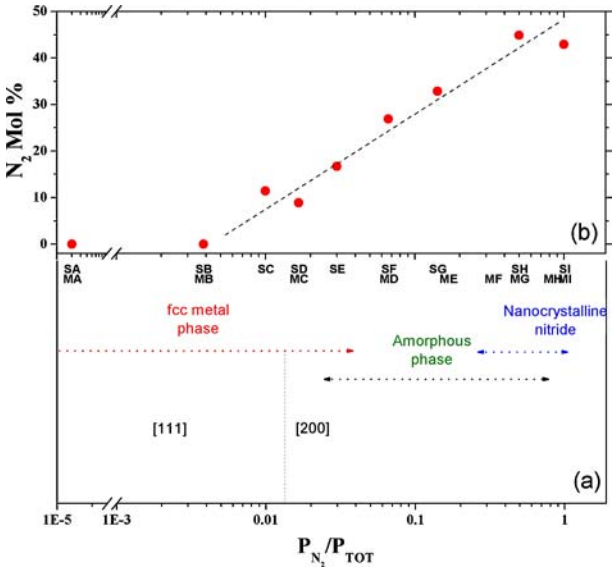

Figure 5 Ranges of existence of the various phases (crystalline metal, amorphous, nanocrystalline nitride) (a) and experimental nitrogen content (b) as a function of the relative nitrogen pressure in the reactive deposition atmosphere for the specimens investigated here. Data are relative to the samples deposited on a silicon substrate (Sa to SI). Samples deposited on AISI D2 are also shown (MA to MI).

with nitrogen pressures around values of samples SE and SH, respectively. It is also interesting to note that the actual nitrogen composition given by EDS approaches 45% above $P_{N_2}/P_{TOT} \approx 0.3 \div 0.5$, thus approaching a MN composition (where M are metals of the base alloy) as in the CoN nitride. This result agrees quite well with the observed formation of nitride phase in samples SH-SI. The amorphous phase is formed for a nitrogen composition in the range $\sim$15% $\div$ $\sim$35%. In particular, sample SF has a nominal composition M_2N, in good agreement with previous results [5]. Concentrations below $\approx$15% seem compatible with the formation of the *fcc* metal phase, which means incorporation of nitrogen as interstitial in a supersaturated solid solution of the alloy elements. Texture evolution from [111] to predominantly [200] is observed above $\approx$ 10% N_2.

The above results are obtained irrespective of the substrate (silicon wafer, stainless steel or glass [10]). For convenience Fig. 5 also reports the compositions of the thin film series deposited on AISI D2 substrates, discussed in the following section.

3.2. Scratch test

Scratch test results are strongly related to the deposition atmosphere and phase composition of the thin films. In particular, coatings show an increasingly fragile behaviour as the nitrogen content in the deposition atmosphere increases. We can define three kinds of coating damages in dependence on the nitrogen content. Coatings deposited in Ar atmosphere (sample MA) show a plastic behaviour. Among the series of coatings presented here, they were the only ones that could be

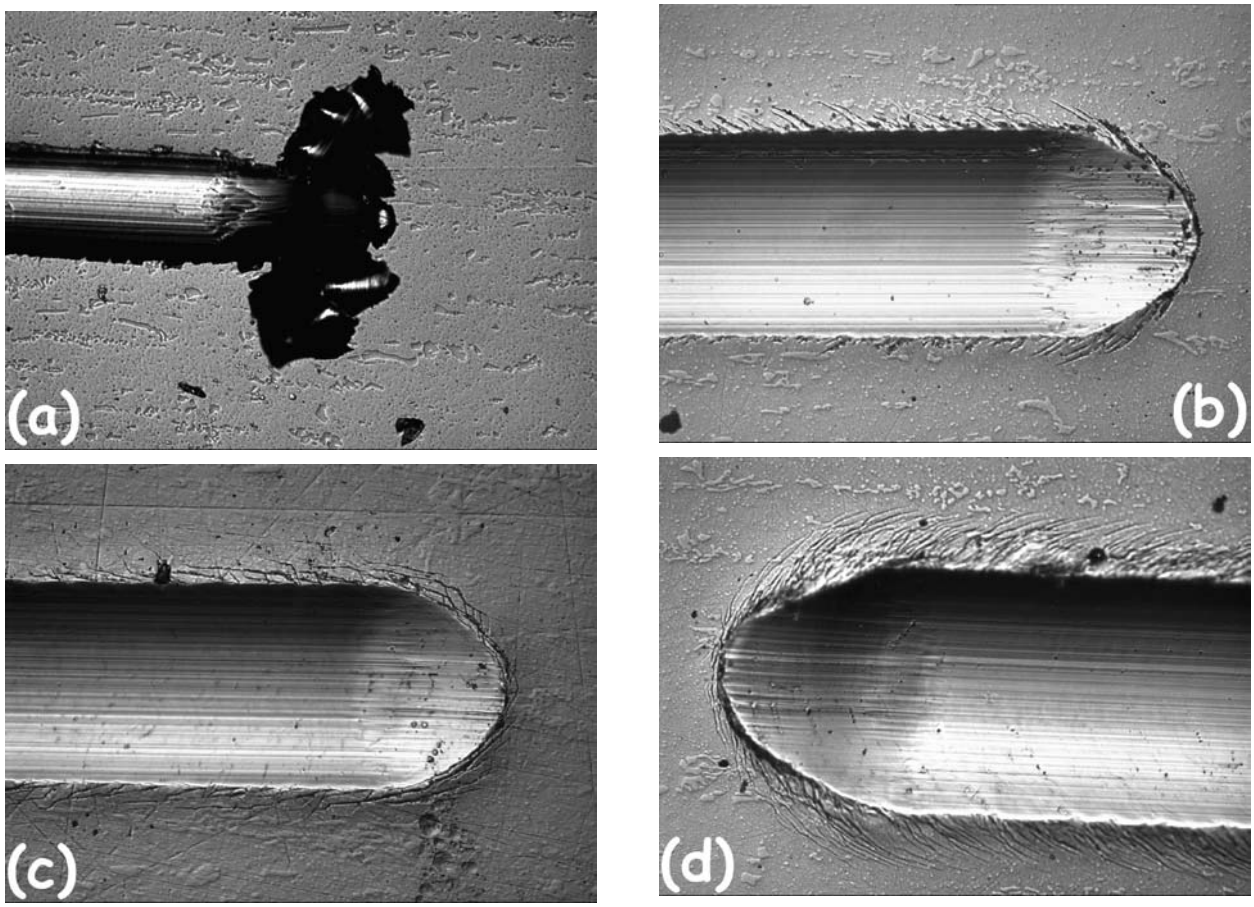

Figure 6 Optical micrographs showing the scratch test results for the films deposited on steel. Detail of the end of a scratch test track for specimens: (a) MA, (b) MB, (c) MC, (d) MD, (e) ME and details of the micro-cracking and delamination occurring in specimens (f) MF, (g) MG, (h) MH, (i) MI. (*Continued.*)

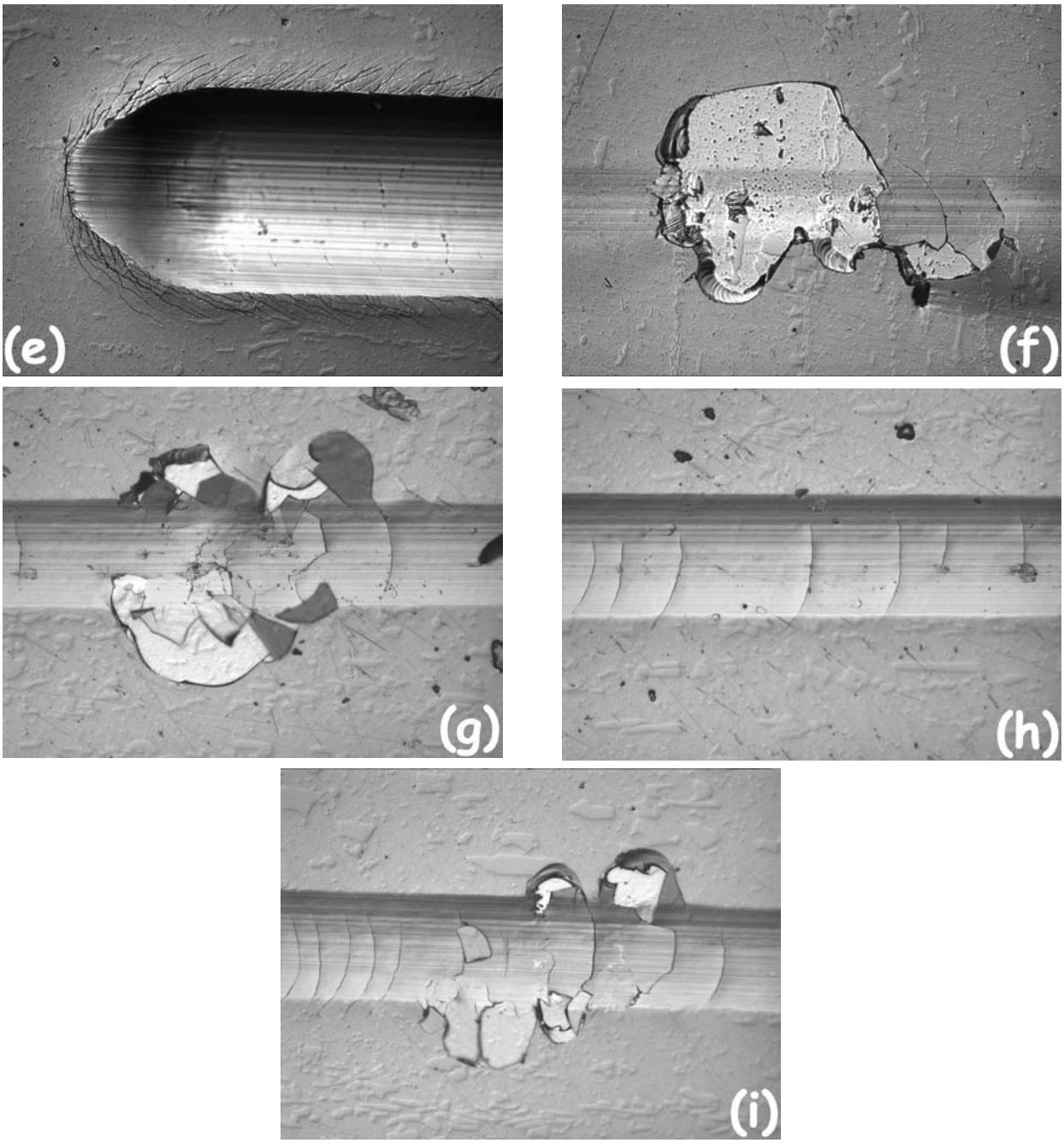

Figure 6 (*Continued.*)

plastically removed from the track at high values of normal force (100 N) (Fig. 6a). For lower values of the normal force, e.g. 0–60 N, the scratch track doesn't show any delamination of the coating, which, instead, appears as still adherent inside the track throughout the test. No cracks are visible inside the track, but an increasing removal of material is noted, and ridges form along the sides of the track owing to the plastic deformation. Ridge generation is likely to produce high tensile stresses in the coating.

At normal force ∼40 N, cracks parallel to the scratch start propagating along a direction perpendicular to coating surface. At higher normal force values (∼70 N) the tensile stresses produced by the ridge formation generate a sequence of cracks inside the ridge itself at a certain angle to the scratch direction (Fig. 6b).

The behaviour of MB and MC coatings is similar to that of sample MA, except that no material was removed from the scratch track even at the highest values of normal force (∼100 N), as visible in Fig. 6c.

Starting from sample MD ($P_{N_2} = 0.4 \times 10^{-1}$ Pa), microscope observation reveals the generation of tensile cracking inside the track, perpendicular to the scratch direction. This feature becomes increasingly visible in the following samples (ME to MI), and tends to appear to lower normal force as the nitrogen content increases (Fig. 6d). Samples MD and ME display an intermediate behaviour between the more plastic (samples MA, MB, MC) and the more fragile coatings (samples MF, MG, MH, MI). For these coatings we do not observe any delamination even at 100 N normal force, nor material loss inside the scratch track, but plastic formation of the ridges with cracks appearing inside the track (perpendicular to the scratch direction) and around the rim of the scratch track (Fig. 6e).

Delamination in samples MF, MG, MH, MI occurs at many points, starting from the cracks formed inside the track in direction perpendicular to the scratch. These cracks have a marked effect on adhesion, and coatings tend to come off from the substrate leaving large regions uncovered around the crack (Fig. 6f–h). Even if coating detachment first starts inside the scratch track, the effective removal of the coating takes place most frequently at the track edge (Fig. 6i). This behaviour is typical of hard fragile coatings such as TiN, CrN etc. [11, 12].

The AE in samples MA, MB, MC, MD and ME starts as soon as the stylus begins moving on the sample surface, and keeps constant to low values during the test. AE for samples MF, MG, MH, MI is more typical of fragile coatings: even if it increases continuously during the scratch test, it shows peaks when largest delaminations occur.

The above observations are justified by the phase composition determined by diffraction (Fig. 5). In fact, samples MA, MB and MC, that show a similar plastic behaviour, are all made of a *fcc* metal phase, with a texture progressively turning from [111] to [200]. The increased resistance of MB and MC with respect to MA, underlines the positive role of nitrogen, tending to reduce domain size and turning the sharp [111] texture of MA progressively into a two component ([200]/[111]) fibre texture in MC. Samples MF, MG, MH and MI show a brittle behaviour, probably resulting from the progressive increase of the nitride phase.

Samples MD and ME exhibit an intermediate and particularly favourable behaviour, as they combine good scratch resistance, with no delamination up to 100 N normal force, with a high hardness (as observed for this range of nitrogen content [5]). These properties are clearly resulting from the fact that the thin films are made of amorphous phase, whose behaviour combines the properties of hard nitrides and amorphous metals, offering interesting perspectives for applications in wear resistant coatings, as top coatings or intermediate buffer layers between metal substrates and hard nitride/carbide layers.

4. Conclusion

Thin films deposited from a CoNiCrAlY alloy target by r.f. Magnetron Sputtering in reactive Ar/N_2 atmosphere show different microstructures and phase compositions as a function of the nitrogen content. Three main phases can be distinguished.

- At low nitrogen partial pressure (up to $\sim 1 \times 10^{-2}$ Pa) a supersaturated solid solution of the alloy elements forms with a *fcc* metal structure, and interstitial nitrogen that reaches a concentration of 10–15%. The metallic thin films are strongly oriented, with a fibre texture (i.e., presence of an orientation axis along the growth direction and absence of any order within the growth plane). At low N_2 concentrations texture is [111] (close packing planes parallel to the surface), whereas for increasing nitrogen content domain size of the metal phase decreases and texture becomes progressively less sharp and turns into a prevailing [200] fibre component. These thin films show a typically plastic behaviour, with an increasingly better resistance to the scratch test for increasing nitrogen concentration.
- Higher nitrogen partial pressures ($PN_2 > 1 \times 10^{-2}$ Pa) lead to the formation of amorphous thin films, with a nitrogen content around a composition M_2N (where M stands for the various metal alloy elements). Properties are quite interesting: these thin films show a good resistance to the scratch test and in any case fail in a plastic mode, similar to some extent to the behaviour of metallic layers.
- Finally, rfMS in nitrogen rich atmosphere (above $\sim 1 \times 10^{-1}$ Pa) promotes the formation of nanocrystalline nitride with a composition close to MN. These thin films exhibit a prevailing brittle behaviour.

It is worth noting that two-phase systems can be produced in suitable ranger of nitrogen partial pressure. Nanocomposite thin films made of a nanocrystalline *fcc* metal phase embedded in an amorphous phase can be deposited for nitrogen partial pressures around $PN_2 \approx 0.18 \times 10^{-1}$ Pa. For higher pressures (of the order of 0.1–0.2 Pa and above) the amorphous phase is present together with a nanocrystalline nitride phase. Future development of this research will address these nanocomposite systems. In particular, thermal stability, phase evolution with the temperature and magnetic properties will be the object of further studies.

Acknowledgements

The present work was supported by the basic research fund of the Italian Ministry of University and Research, project FIRB, "Wear-resistant nanocrystalline coatings". Authors are grateful to the colleagues F. Branda and G. Luciani of the University of Napoli for the EDS data.

References

1. S. VEPŘEK, *J. Vac. Sci. Technol. A* **17**(5) (1999) 2401.
2. S. ZHANG, D. SUN, Y. FU and H. DU, *Surf. Coat. Technol.* **167** (2003) 113.
3. J. MUSIL, *Mat. Chem. Phys.* **54** (1998) 116.
4. *Idem.*, *Surf. Coat. Technol.* **125** (2000) 322.
5. P. SCARDI, Y. H. DONG and C. TOSI, *J. Vac. Sci. Technol. A* **19**(5) (2001) 2394.
6. P. SCARDI and Y. H. DONG, *J. Mater. Res.* **16**(1) (2001) 233.
7. P. SCARDI, M. LEONI and Y. H. DONG, *Adv. X-ray Anal.* **42** (2000) (On CD-ROM).
8. International Centre for Diffraction Data, 12 Campus Boulevard, Newtown Square, PA (USA). PDF2 card #83-831.
9. M. LEONI, U. WELZEL and P. SCARDI, *J. Res. Natl. Inst. Stand. Technol.* **109** (2004) 27.
10. P. SCARDI, M. LEONI, G. AUSANIO, V. IANNOTTI and L. LANOTTE, *Appl. Phys. A* (2005) in press.
11. S. J. BULL, *Tribol. Intern.* **30**(7) (1997) 491.
12. P. HEDENQVIST and S. HOGMAN, *ibid.* **30**(7) (1997) 507.

Received 21 November 2003
and accepted 8 November 2004